Available online at www.sciencedirect.com
ScienceDirect
Trans. Nonferrous Met. Soc. China 32(2022) 354−363
Transactions of Nonferrous Metals Society of China
www.tnmsc.cn

Improving corrosion resistance of Cu−Al-based anodes in KF−AlF_3−Al_2O_3 melts

Sai Krishna PADAMATA[1], Andrey YASINSKIY[1], Aleksandr SHABANOV[2], Timofey BERMESHEV[1], You-jian YANG[3], Zhao-wen WANG[3], Dao CAO[3], Peter POLYAKOV[1]

1. Laboratory of Physics and Chemistry of Metallurgical Processes and Materials, Siberian Federal University, Krasnoyarsk, Russia;
2. Laboratory of Molecular Spectroscopy, Krasnoyarsk Science Center SB RAS, Krasnoyarsk, Russia;
3. School of Metallurgy, Northeastern University, Shenyang 110819, China

Received 17 February 2021; accepted 30 July 2021

Abstract: The anodic behaviour of pre-oxidised and non-oxidised Cu−Al-based anodes (Cu−10Al and Cu−9.8Al−2Mn) in KF−AlF_3−Al_2O_3 melts was studied through galvanostatic and potentiodynamic polarization techniques. The alloy compositions were oxidised for a short-term (8 h) at 700 °C, followed by galvanostatic polarization for 1 h at 800 °C with an applied current density of 0.4 A/cm^2. The potentiodynamic curves were recorded with a sweep rate of 0.01 V/s. XRD analysis was conducted on frozen melt samples collected on the surface of the anode, and SEM observation was performed on the anode after the experiment to study the phases of the scales formed on the alloys. All the anode materials had a steady potential between 2.30 and 2.50 V (vs Al/AlF_3). The corrosion rates of the anodes were calculated from the data acquired through potentiodynamic polarization. It was seen that pre-oxidised anodes possess a low corrosion rate compared to those without pre-oxidation treatment.

Key words: inert anodes; potassium cryolite; Cu−Al alloys; corrosion; aluminium electrolysis; oxygen-evolving electrodes

1 Introduction

According to the Hall−Heroult process, aluminium electrolysis is performed by using consumable carbon anode (blocks) and aluminium liquid cathode. It is well established that consumable carbon anodes contribute to the emission of high amounts of carbon dioxide and perfluorocarbons, and the process requires high energy consumption [1]. The principle reactions occurring in the Hall−Heroult process causing the emission of byproducts at 1000 °C are as follows:

$$Al_2O_{3(diss)}+3/2C_{(s)}=2Al_{(l)}+3/2CO_{2(g)}$$
(Standard EMF φ^{Θ}=1.168 V) (1)

$$Al_2O_{3(diss)}+3C_{(s)}=2Al_{(l)}+3CO_{(g)}\ (\varphi^{\Theta}=1.033\ V) \quad (2)$$

$$2AlF_{3(diss)}+2C_{(s)}=2Al_{(l)}+C_2F_{6(g)}\ (\varphi^{\Theta}=2.378\ V) \quad (3)$$

$$4AlF_{3(diss)}+3C_{(s)}=4Al_{(l)}+3CF_{4(g)}\ (\varphi^{\Theta}=2.155\ V) \quad (4)$$

Moreover, around 14.4 t of CO_2 is emitted (including the indirect contribution from the electric power used in the process) per ton of aluminium production. For the past four decades, a considerable amount of research has been conducted to develop suitable inert anode materials such as cermets, ceramics and metals [2−7]. The following reaction takes place when inert anodes are used:

$$Al_2O_{3(diss)}=2Al_{(l)}+3/2O_{2(g)}\ (\varphi^{\Theta}_{750\ ^{\circ}C}=2.337\ V) \quad (5)$$

The Ni−Fe-based metallic alloys are widely

Corresponding author: Sai Krishna PADAMATA, E-mail: saikrishnapadamata17@gmail.com
DOI: 10.1016/S1003-6326(22)65800-X

regarded as the promising candidate to be an inert anode material. They are considered stable materials because of the corrosion resistive oxide scale ($Ni_xFe_{3-x}O_4$) formed on the outer surface in the cryolite melt [8,9]. Other than the Ni−Fe-based metallic inert anodes, Cu−Ni−Fe-based [10−12] and Cu−Al-based [13,14] alloys have also shown prominence. The Cu−Al-based anode has been tested in potassium cryolite melts and alumina suspensions at different parameters, and promising results have been achieved [15,16]. The CuO, Cu_2O, $CuAlO_2$ and $CuAl_2O_4$ oxide scales formed on the Cu−Al electrode surface improve corrosion resistance. It is also well established that copper aluminate scales have low solubility in cryolite−alumina melt, which means that anode products do not contaminate the melt and aluminium metal. Furthermore, the oxide layers formed on the aluminium bronze alloy exhibit high electrical conductivity. The high melting point of the aluminium bronze alloy can withstand electrolyte overheating, enabling the process without any thermal shocks [17].

The oxide scale must be self-repairing, and the oxide dissolution rate should be equal to or less than the oxide replenishment rate. In general, the anodic reaction depends upon the electrochemical potential. For example, when the electrochemical potential is less than the oxygen evolution potential (2.2 V) but greater than the metal oxidation potential, the following reaction will take place:

$$a\mathrm{M}_{(s)}+b\mathrm{O}^{2-}_{(diss)}=\mathrm{M}_a\mathrm{O}_b+2b\mathrm{e}^- \quad (6)$$

When the electrochemical potential is greater than both the metal oxidation and oxygen potentials, the following relation will take place:

$$a\mathrm{M}_{(s)}+b/2\mathrm{O}_{2(g)}=\mathrm{M}_a\mathrm{O}_{b(s)} \quad (7)$$

A decrease in the operating temperature of the electrolysis process can be considered inert anode friendly as it reduces the corrosion rate of the anode material and the thermal shocks, and provides easy operational conductions. $KF-AlF_3$ melts can be used as a low-temperature bath as they possess low liquidus temperature (depending upon the cryolite ratio (CR, molar ratio of KF to AlF_3). The eutectic temperature of the $KF-AlF_3$ melt is only 580 °C, which is lower compared to the eutectic temperature of $NaF-AlF_3$ melt (700 °C). The potassium cryolite melt has a higher alumina solubility and a higher dissolution rate than sodium cryolite melt at a similar temperature [18,19]. A low operating temperature could avoid fluorine penetration in the cathode and cell lining [20]. However, alumina is evenly distributed in the bath at high temperatures [21], so it is advantageous to have an operating temperature at around 800 °C while using $KF-AlF_3$ melts.

The parameters of the studies such as CR, working temperature and anode composition were based on the previous results obtained, where the current efficiency was around 84.4% and the produced aluminium purity was 99.4% [17]. The importance of this work is to understand the influence of pre-oxidation on the anode process of the alloy. It is known that pre-oxidising the anode can improve corrosion resistance and chemical stability [22]. A small percentage of Mn was added to the Cu−Al alloy as Mn increased the corrosion resistance when combined with CuO oxide [23].

In this work, the corrosion resistance of Cu−Al and Cu−Al−Mn alloys in $1.4KF-AlF_3-Al_2O_3$ melt was investigated at 800 °C. The alloys with and without pre-oxidation treatment were tested by short-term galvanostatic polarization and potentio-dynamic polarization. The anode samples after the polarization were examined using the scanning electron microscopy method to understand the oxide layer formation. In addition, the frozen electrolyte on the surface of the alloys was collected for performing X-ray diffraction measurement to understand the contamination of metal in the melt.

2 Experimental

2.1 Alloy preparation

Thin-rod shaped Cu−Al-based anodes with two compositions Cu−10Al and Cu−9.8Al−2Mn (wt.%) were prepared in a vacuum induction furnace at 1050 °C. The materials used had a purity of 99.95% Cu, 99.99% Al and 99.95% Mn. The alloys were cast into rods using a steel crucible with a rod-shaped mould (diameter: 5 mm; length: 50 mm). The alloys (Cu−Al and Cu−Al−Mn) were pre-oxidised at 700 °C for 8 h before the galvanostatic polarisation. A 3 mm-diameter hole was drilled on alloy, and threading was made to introduce stainless steel rod, which acted as a current lead. The nominal compositions of the alloys are shown in Table 1.

Table 1 Compositions of anode materials tested in potassium cryolite melt

Alloy	Anode condition	Mass fraction/%		
		Cu	Al	Mn
Cu−10Al	Non-oxidised	90.0	10.0	0
Cu−10Al	Pre-oxidised	90.0	10.0	0
Cu−9.8Al−2Mn	Non-oxidised	88.2	9.8	2.0
Cu−9.8Al−2Mn	Pre-oxidised	88.2	9.8	2.0

The pre-oxidised specimens contain oxygen on the active surface, where the contents of oxygen on pre-oxidised Cu−Al and Cu−Al−Mn are 3.43 at.% and 0.37 at.%, respectively

2.2 Electrolyte preparation

The electrolyte was prepared from two individual salts KF and AlF_3, both reagent grades supplied by Reachim (Russia). Initially, the salts were dried at 400 °C to remove the moisture. Then, the cell was heated at a rate of 120 °C/h. The dried salts with the CR (1.4) were transferred to the graphite crucible and heated at 850 °C to liquidise. Finally, alumina (5 wt.%) was added to the KF−AlF_3 melt to keep the melt saturated. Before the tests, the electrolyte was refined by performing a potentiostatic process where the graphite working electrode was used, and a potential of 0.2 V (vs Al/AlF_3) reference electrode was applied. The process was performed for 2 h (or till the current reached 0).

2.3 Electrochemical measurements and materials characterisation

The studies were performed on the vertical three-electrode cell, as shown in Fig. 1, where a Cu−Al thin cylindrical rod was used as a working electrode (WE). The graphite crucible acted as the counter electrode. The WE potential was measured versus the liquid aluminium reference electrode. Autolab PGSTAT302n potentiostat instrument and Nova 2.1.2 software (The MetrOhm, Netherlands) were used to obtain potentiodynamic and Galvanostatic polarization curves. The cell temperature was measured with a K-type thermocouple, and the USB-TC01 thermocouple module was used to maintain a constant value (±3 °C). X-ray diffraction technique was performed on the frozen salt samples collected on the alloys after the galvanostatic polarization to understand melt contamination by the anode corrosion products. The process was carried out using an X′Pert PRO diffractometer with a PIXcel detector equipped with Cu $K_{\alpha 1,2}$ radiation and graphite monochromator. The HT1200 (AntonPaar) camera was used to scan the diffraction patterns under high temperature and vacuum. XRD patterns were recorded in the 2θ range of 2°−62° with a step of 0.03°. SIROQUANT package was used to estimate the oxide percentage from the total phase compositions. The SEM−EDX analysis was performed using Hitachi TM4000, Hitachi SU3500 electron microscopes and the elemental mapping was done using the BRUKER Xflash 410 detector.

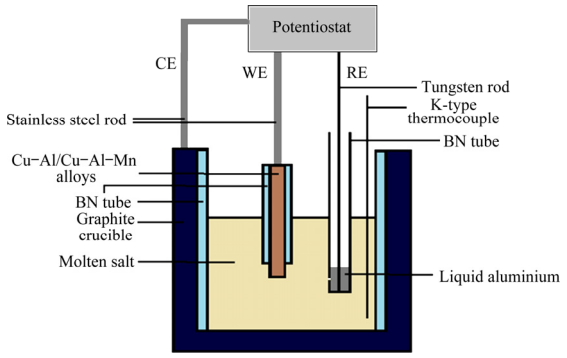

Fig. 1 Schematic drawing of experimental setup

3 Results and discussion

3.1 Short-term galvanostatic polarization

The open-circuit potentials (OCP) were recorded versus the Al/AlF_3 reference electrode once the WE was immersed in the melt. The difference in the OCP of the non-oxidised and pre-oxidised alloys reveals the presence of oxide on the surface of the alloy. The alloy with 2 wt.% addition of Mn has higher OCP, indicating that the alloy has high corrosion resistance. The pre-oxidised Cu−9.8Al−2Mn alloy has lower OCP compared to the pre-oxidised Cu−10Al alloy. We assume that the introduction of the Mn could have reduced the thickness of the scale formed on the alloy. The OCP values are presented in Table 2.

The potential versus time plots for the galvanostatic polarization process are shown in Fig. 2. The applied current density was 0.4 A/cm^2. The total potential φ_i which is the potential difference between the WE and the RE, is the sum of anodic over potential η_a, ohmic voltage drop and anode reversible potential φa relative to the RE. The following equation represents the total potential:

Table 2 OCP values for non-oxidised and pre-oxidised Cu−10Al and Cu−9.8Al−2Mn anodes

Anode	OCP (vs Al/AlF_3)/V	
	Non-oxidised	Pre-oxidised
Cu−10Al	0.19	1.27
Cu−9.8Al−2Mn	0.31	1.03

$$\varphi_i=\eta_a+IR+\varphi_a \quad (8)$$

where I is the current applied and R is the total electric resistance.

The total electric resistance is around 500 mΩ (obtained from the *i*-interrupt method), and the applied current is 0.216 A which makes ohmic voltage drop to be around 0.108 V. The η_a is close to 0.2 V, so the remaining potential for all the cases is between 2.00 and 2.20 V and is associated with the reversible potential. It is difficult to precisely predict the exact reactions occurring on the anode surface due to the presence of active species like oxyfluoroaluminates ($AlOF_2^-$, $Al_2OF_6^{2-}$ and $Al_2O_2F_4^{2-}$) and aluminium fluorides (AlF_4^- and AlF_6^{3-}) in the cryolite melts [18]. In Ref. [24], it has been indicated that the gaseous $AlOF_2$ is simultaneously generated along with the O_2 gas due to the oxidation of $AlOF_2^-$ complex ions. In general, it is difficult to predict the exact reaction occurring at a certain point in time as it is also well known that simultaneous oxides are formed at a given instant.

To compare the non-oxidised and pre-oxidised anodes behaviour at given constant parameters (0.4 A/cm^2, 800 °C), keen observation is required on the potential difference between the anode material (WE) and the RE. Figures 2(a, b) shows the closer view of the galvanostatic polarization for the first 10 min. The Cu−10Al anodes, both pre-oxidised and non-oxidised, require less time than pre-oxidised and non-oxidised Cu−9.8Al−2Mn, which shows that the Mn plays a crucial role in the formation of the oxide scale while only having 2 wt.% of the total composition of the alloy.

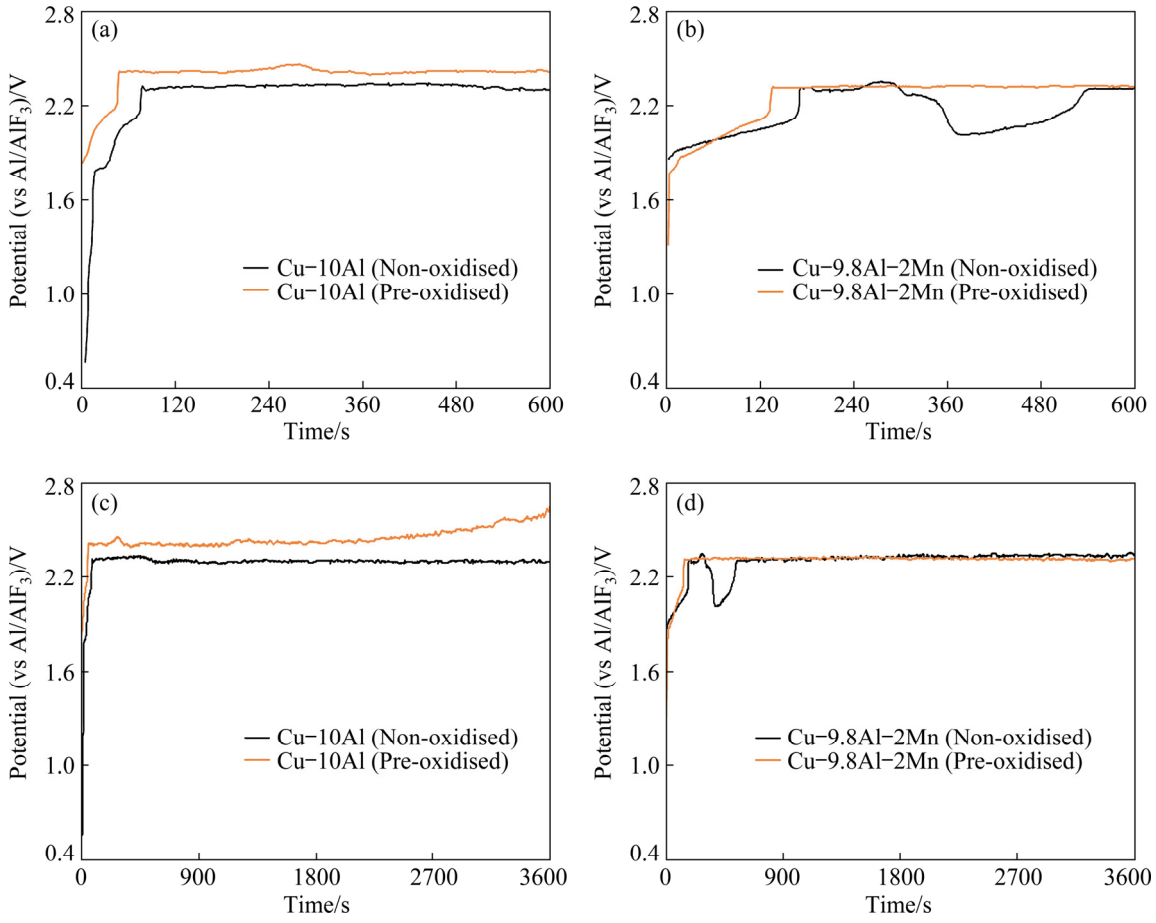

Fig. 2 Potential versus time plots for non-oxidised and pre-oxidised Cu−10Al (a, c) and Cu−9.8Al−2Mn (b, d) electrodes at 0.4 A/cm^2 and 800 °C: (a, b) Close-up view of initial galvanostatic polarization period; (c, d) Full galvanostatic polarization period

In the case of the Cu−10Al anode, the steady-state was achieved within 44 s for the pre-oxidised anode compared to the non-oxidised one, which required 77 s. This phenomenon is due to the pre-existing oxide scale on the treated anode, while the bare anode required a bit more time to form the stable oxide phase. A similar scenario can be seen in the case of Cu−9.8Al−2Mn anode, where the pre-oxidised anode required 135 s to attain a steady-state while it took 535 s to obtain a steady-state in the case of non-oxidised Cu−9.8Al−2Mn anode (Figs. 2(c, d)). A gradual drop in the potential difference for non-oxidised Cu−9.8Al−2Mn anode at 285 s is related to the dissolution or a spall of the oxide scale. It took around 250 s to reach steady-state (to form a stable oxide scale) after a drop in potential difference. In both anodes, the pre-oxidised ones had more potential difference compared to the bare anodes. A gradual increase in the potential difference from 2.43 to 2.61 V caused by the potential drop can be seen in the pre-oxidised Cu−10Al anode after 35 min of the polarization until the anode potential difference was in a steady-state. The reason could be the formation of non-conductive oxide scales on the outer surface, which could lead to the passivation of the anode. On the other hand, although it took a bit longer time to reach a steady-state in both pre-oxidised and non-oxidised Cu−9.8Al−2Mn anodes, once the stability in potential difference was attained, it remained steady till the end of the polarization process, which indicates that the decomposition rate of oxides is equal to the formation rate of oxides for Cu−9.8Al−2Mn anodes. The time taken to reach the steady-state is related to the corrosion resistance in the case of Cu−9.8Al−2Mn anode. We can see that the corrosion rate is lower for pre-oxidised while the steady-state is attained quicker compared to the non-oxidised Cu−9.8Al−2Mn anode.

The reversible potential is less than 2.3 V which corresponds to the decomposition of Al_2O_3 and evolution of O_2 as the product of anode. The following reactions could be the source of O_2 evolution on the anode surface:

$$2Cu+Al_2O_3=2Al_{(l)}+2CuO+0.5O_{2(g)} \quad (\varphi^{\Theta}_{800\,^{\circ}C}=2.10\ V) \tag{9}$$

$$5Cu+2Al_2O_3=4Al_{(l)}+5CuO+0.5O_{2(g)} \quad (\varphi^{\Theta}_{800\,^{\circ}C}=2.05\ V) \tag{10}$$

3.2 Potentiodynamic polarization

The potentiodynamic polarization was performed to estimate the corrosion rate of the anode materials. The applied sweep rate was 0.01 V/s in the potential range between −0.5 and 3 V. The curves obtained from the above process are shown in Fig. 3. The process was performed twice to make sure that the recorded curves were constant. The corrosion current density and the corrosion potential were determined from the intersection point of the tangents plotting from the cathodic and anodic curves.

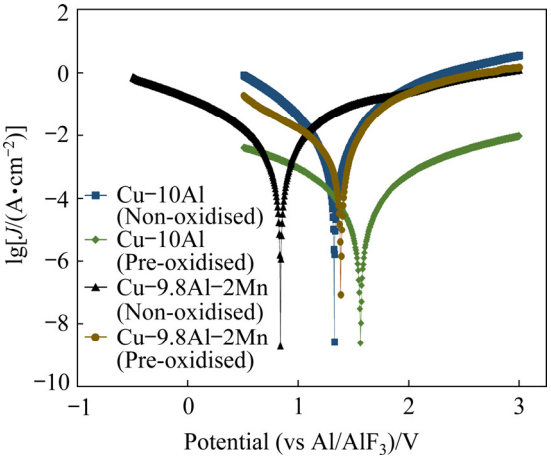

Fig. 3 Potentiodynamic polarization curves at sweep rate of 0.01 V/s for non-oxidised and pre-oxidised Cu−10Al and Cu−9.8Al−2Mn electrodes after 1 h galvanostatic polarization

The corrosion rate was calculated using the below equation:

$$v_{corr}=\frac{3272J_{corr}E_w}{d} \tag{11}$$

where v_{corr} is the corrosion rate in mm/a, J_{corr} is the corrosion current density in A/cm^2, E_w is the equivalent mass of alloy in g (for Cu−10Al: 29.495 and for Cu−9.8Al−2Mn: 29.016), and d is the density of the alloy in g/cm^3 (for Cu−10Al: 7.273 and for Cu−9.8Al−2Mn: 7.249)

The more positive corrosion potential (1.56 V) in Cu−10Al (pre-oxidised) suggests that the alloy is not easily corroded. The pre-oxidised Cu−10Al anode has a low corrosion rate and more positive corrosion potential, suggesting that the anode material is more resistant to corrosion and reflects corrosion rate value. From Table 3, it can be seen that the Cu−10Al (pre-oxidised) has a 90%−95% lower corrosion rate compared to other alloys. This

might be due to the passive layer formation on the anode surface, which attributes to the low corrosion rate.

Table 3 Corrosion parameters of Cu−10Al and Cu−9.8Al−2Mn anodes measured in $KF-AlF_3-Al_2O_3$ (CR=1.4) melt at 800 °C

Anode	J_{corr}/ (mA·cm^{-2})	φ_{corr}/ V	Corrosion rate/ (mm·a^{-1})
Cu−10Al (Non-oxidised)	2.23	1.32	29.59
Cu−10Al (Pre-oxidised)	0.11	1.56	1.45
Cu−9.8Al−2Mn (Non-oxidised)	1.54	0.84	20.16
Cu−9.8Al−2Mn (Pre-oxidised)	1.17	1.38	15.32

3.3 Material characterisation

The frozen melt sample on the anode material was collected after the galvanostatic polarization. The X-ray diffraction method was performed to check the contamination of anode products in the melts. The XRD patterns were recorded in the 2θ range of 2°−62°. The mass of the collected sample was around 2 g. The XRD patterns obtained are shown in Fig. 4. The samples collected on the non-oxidised Cu−10Al anode contained three types of oxides: Cu_2O (1.56 wt.%), CuO (9.96 wt.%), $CuAlO_2$ (0.80 wt.%) and metallic Cu (3.01 wt.%), and the rest of the samples contained melts with different phases such as K_2NaAlF_6, $KAlF_4$, K_3AlF_6 and KAl_4F_{13}. The presence of anode products in the collected samples indicates that the scales formed on the surface are unstable. It might be due to the formation of metal fluoride on the surface of the anode material. In the pre-oxidised Cu−10Al anode, only metallic Cu (0.45 wt.%) was identified in the examined sample due to the low content of the oxidation products.

In samples collected on the non-oxidised Cu−Al−Mn anode, only Cu_2O (0.12 wt.%) was found. While similar to the pre-oxidised Cu−10Al anode, samples collected on the pre-oxidised Cu−9.8Al−2Mn anode also had only metallic Cu (0.54 wt.%) identified by XRD.

The SEM method was used to examine the anode surface after the galvanostatic polarization process. The EDX elemental mapping and single-point analysis were performed to estimate the

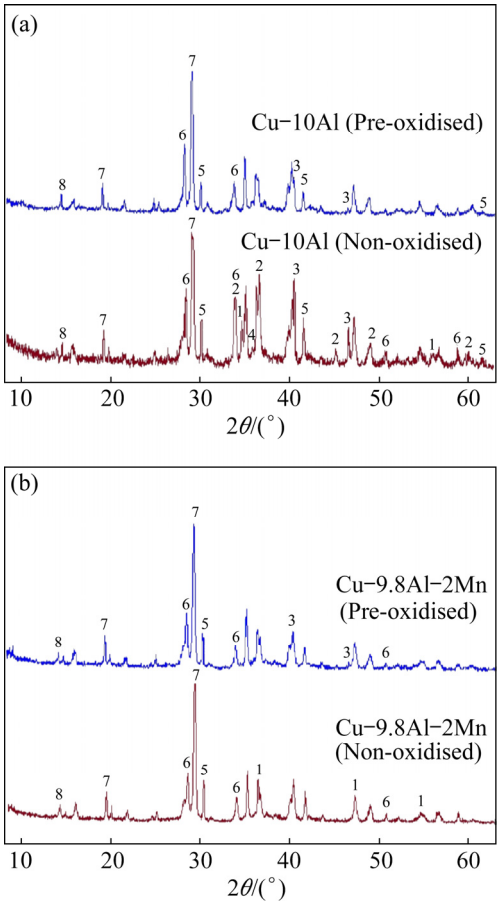

Fig. 4 XRD patterns obtained for samples collected on Cu−10Al (a) and Cu−9.8Al−2Mn (b) anodes after 1 h galvanostatic polarization: 1−Cu_2O; 2−CuO; 3−Cu; 4−$CuAlO_2$; 5−K_2NaAlF_6; 6−$KAlF_4$; 7−K_3AlF_6; 8−KAl_4F_{13}

presence of a particular oxide scale. The SEM cross-section images of non-oxidised and pre-oxidised anodes can be seen in Fig. 5. In general, the metallic oxide is formed as a first scale on the non-oxidised anode when immersed in the fluoride melts, and in this case, according to the elemental mapping, CuF_2 or CuF is supposed to form. Thus, the following two reactions could occur (The Gibbs energy changes for the above reactions are calculated using HSC Chemistry 6.0 software):

$$Cu_{(s)} + AlF_5^{2-} \rightarrow CuF_2 + AlF_3 + 2e^-$$
$$\Delta_r G^{\ominus} = -367.037 \text{ kJ/mol} \quad (12)$$

$$Cu_{(s)} + AlF_4^{-} \rightarrow CuF_2 + AlF_3 + e^-$$
$$\Delta_r G^{\ominus} = -513.279 \text{ kJ/mol} \quad (13)$$

The outer layer is mainly composed of CuO and Cu_2O. The brighter spots in the image represent the Cu metal. The darker spots (Zones 4 and 5 in

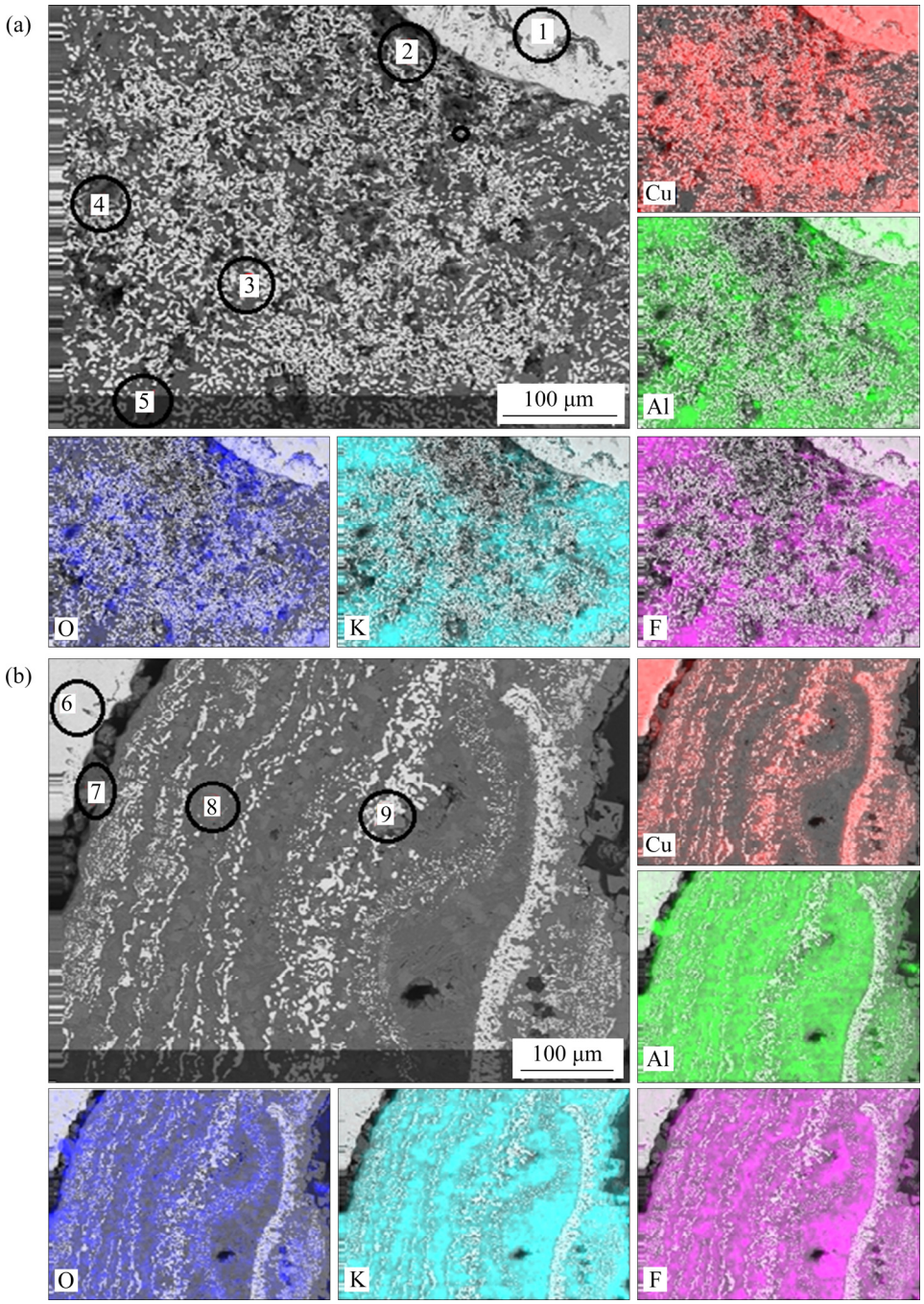

Fig. 5 SEM−EDX images of cross-section of Cu−10Al anode after 1 h galvanostatic polarization: (a) Non-oxidised; (b) Pre-oxidised

Fig. 5(a)) contain a high content of fluorine, which might be the electrolyte and copper fluoride. In the pre-oxidised Cu−10Al anode, a pre- existing scale can be seen in Zone 7 of Fig. 5(b). Unlike the bare Cu−10Al anode where the metal fluorides are formed, the first layer on the anode surface comprises metallic oxides such as CuO, Cu_2O and $CuAlO_2$. In this pre-oxidised Cu−10Al anode, a presence of significant fluorine content can be seen (Zone 8 in Fig. 5(b)), while Zone 9 in Fig. 5(b) contains copper-based oxides and some electrolyte content. A gradual increase in the potential difference in the galvanostatic polarization curves could be due to the presence of electrolyte between the outer layer and the pre-existing scale. The single-point analysis data can be seen in Table 4.

The SEM images of the cross-sections of the Cu−9.8Al−2Mn (both non-oxidised and

Table 4 Contents of elements on cross-section of anode and in melt in Fig. 5 using SEM−EDX single-point analysis

Zone No.	Content/at.%					Total content/ at.%
	Cu	Al	O	K	F	
1	82.38	17.62	0	0	0	100
2	19.78	13.26	33.32	9.37	24.27	100
3	54.83	13.78	21.21	6.00	4.18	100
4	19.23	8.84	43.13	7.70	21.10	100
5	4.93	16.57	11.44	16.81	50.25	100
6	78.77	17.79	3.43	0	0	100
7	41.85	28.31	24.62	2.03	3.20	100
8	3.19	17.73	14.60	20.26	44.22	100
9	44.60	17.06	13.21	10.28	17.85	100

pre-oxidised) anodes can be seen in Fig. 6. The single-point analysis data can be seen in Table 5. It is surprising to see that the first layer (Zone 2 in Fig. 6(a)) on the non-oxidised anode is metallic oxide rather than a non-conducting metal fluoride scale. The darker portions (Zone 3 in Fig. 6(a)) in this image have a high fluorine content and are possibly melt, and Zone 4 in Fig. 6(a) is a metallic oxide that might also contain MnO and MnO_2.

In the pre-oxidised Cu−Al−Mn anode, an oxide scale formed due to the oxidation process can be seen in Zone 7 in Fig. 6(b), visibly differentiated from other layers. Multiple layers of metallic oxides and electrolyte content can be seen in Fig. 6(b),

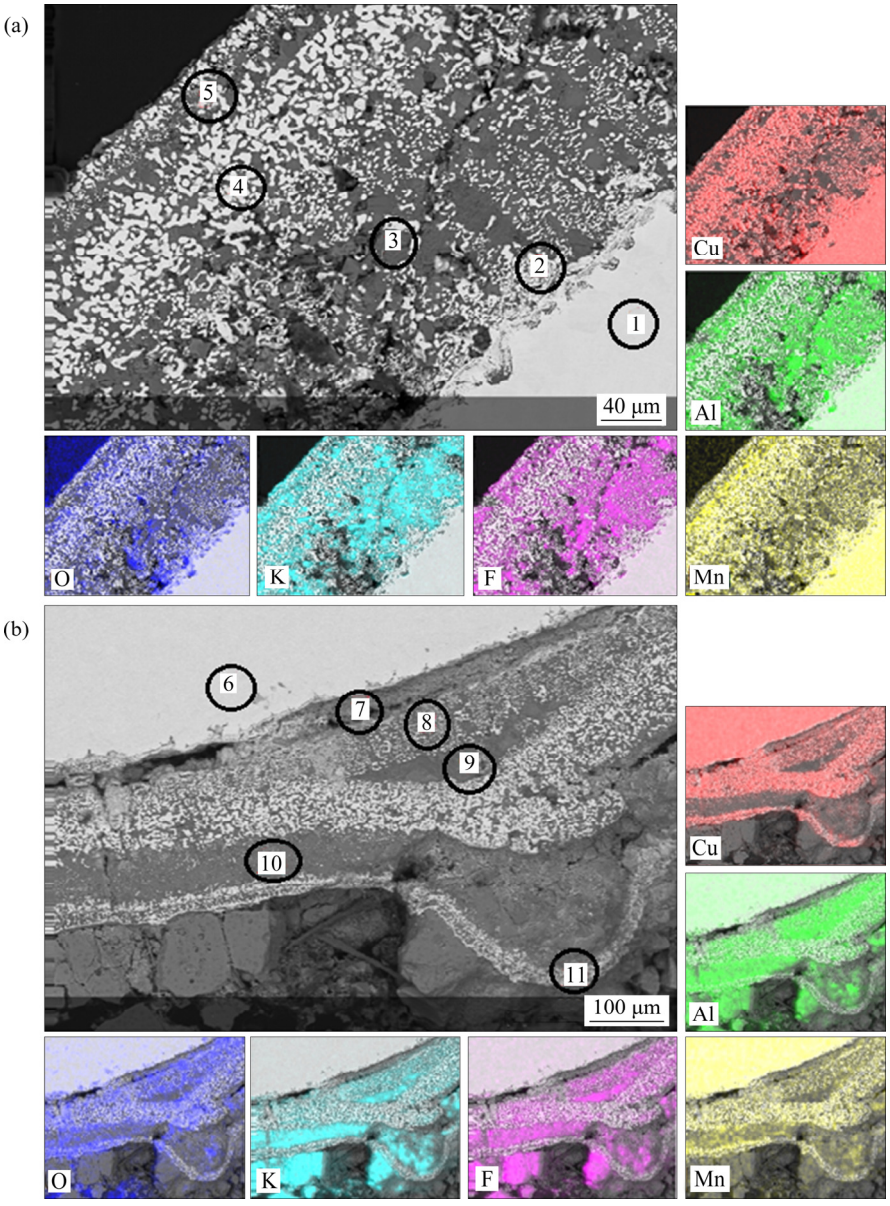

Fig. 6 SEM−EDX images of cross-section of Cu−9.8Al−2Mn anode after 1 h short galvanostatic polarization: (a) Non-oxidised; (b) Pre-oxidised

Table 5 Contents of elements on cross-section of anode and melt in Fig. 6 obtained using SEM−EDX single-point analysis

Zone No.	Content/at.%						Total content/ at.%
	Cu	Al	Mn	O	K	F	
1	80.63	17.93	1.45	0	0	0	100
2	64.97	8.23	0.98	17.06	2.14	6.64	100
3	3.27	16.58	0.03	12.35	15.69	52.08	100
4	59.07	11.93	0.35	14.78	5.85	8.03	100
5	26.78	16.79	0.12	12.22	14.65	29.43	100
6	80.84	16.54	2.25	0.37	0	0	100
7	43.40	12.71	1.29	28.42	10.36	3.82	100
8	32.25	16.78	3.08	21.73	11.06	15.10	100
9	2.98	17.41	0.09	9.65	18.93	50.94	100
10	3.43	13.32	0.40	15.41	20.58	46.79	100
11	38.68	10.97	3.16	18.51	18.37	10.31	100

where Zones 8 and 11 contain metallic oxides and a significant amount of Mn relative to its content in the alloy.

Compared to the Cu−10Al anodes, Cu−9.8Al−2Mn anodes had a lower potential difference and attained steady-state till the end of the process, although more time was needed to obtain constant potential. The presence of Mn in anode samples has played a crucial role in the stability of cell potential, which might be due to the absence of metal fluoride formation as the primary oxide layer, unlike the case of Cu−10Al alloy (non-oxidised and pre-oxidised) where metal fluorides are readily formed.

4 Conclusions

(1) The potential difference of all the anodes vs Al reference electrode (during the galvanostatic polarization) was in the range of 2.30−2.50 V, and the steady-state was attained earlier in anodes with pre-oxidation.

(2) The corrosion rates of the pre-oxidised anodes are lower compared to those of non-oxidised ones, and pre-oxidised Cu−10Al has a corrosion rate of 1.45 mm/a, which is 90%−95% lower compared to that of the other three anodes. This could be due to the passivation of the anode from the formation of Al_2O_3 and $CuAl_2O_4$ layers on the pre-oxidised Cu−10Al anode.

(3) SEM results show that the metal fluoride is formed as the first layer on the non-oxidised Cu−10Al anode, which is expected. Still, the non-oxidised Cu−9.8Al−2Mn does not contain any metal fluoride, which is unusual.

(4) The presence of Mn in the Cu−10Al alloy results in a steady state during the polarization process for a longer period. At the same time, the corrosion rate of pre-oxidised Cu−10Al anode is lower compared to that of the pre-oxidised Cu−9.8Al−2Mn anode.

(5) The Cu−9.8Al−2Mn anodes (both non-oxidised and pre-oxidised) show promising performance, and long-term electrolysis must be conducted to see the performance.

Acknowledgments

The work is performed as a part of the State Assignment for the Science of Siberian Federal University, Russia (No. FSRZ-2020-0013). Use of Krasnoyarsk Regional Center of Research Equipment of Federal Research Center “Krasnoyarsk Science Center SB RAS” is acknowledged.

References

[1] ROBINSON T. Lowering energy intensity and emissions in the aluminium industry with government/industry/academia partnership [C]//Light Metals. Warrendale, PA, USA: TMS, 2004: 277–281.

[2] PAWLEK R P. Inert anodes for the primary aluminium industry: An update [C]//Light Metals. Warrendale, PA: TMS, 1996: 243−248.

[3] CAO D, MA Y F, SHI Z N, XU J L, HU X W, WANG Z W. Performance of protective oxide films on Fe–Ni alloy anodes in molten KF–AlF_3–Al_2O_3 salts at 700 °C [J]. Electrochimica Acta, 2020, 347: 136275.

[4] JUCKEN S, MARTIN M H, IRISSOU E, DAVIS B, GUAY D, ROUÉ L. Cold-sprayed Cu−Ni−Fe anodes for CO_2-free aluminum production [J]. Journal of Thermal Spray Technology, 2020, 29(4): 670−683.

[5] YING L, DENGPENG C, WEI W, DONGSHENG L, JUNWEI W, YUDONG L, ZHIRONG S. Influences of heat treatment on the oxidation and corrosion behaviour of Cu−Ni−Fe inert anodes for aluminium electrolysis [J]. Journal of Alloys and Compounds, 2020, 832: 154848.

[6] PAWLEK R P. Inert anodes: An update [C]//Light Metals. Warrendale, PA: TMS, 2014: 1309−1313.

[7] YASINSKIY A S, PADAMATA S K, POLYAKOV P V, SHABANOV A V. An update on inert anodes for aluminium electrolysis [J]. Non-ferrous Metals, 2020, 48: 15−23.

[8] OLSEN E, THONSTAD J. Nickel ferrite as inert anodes in aluminium electrolysis: Part I. Material fabrication and preliminary testing [J]. Journal of Applied Electrochemistry,

1999, 29: 293−299.
[9] OLSEN E, THONSTAD J. Nickel ferrite as inert anodes in aluminium electrolysis: Part II. Material performance and long-term testing [J]. Journal of Applied Electrochemistry, 1999, 29: 301−311.
[10] GAVRILOVA E, GOUPIL G, DAVIS B, GUAY D, ROUÉ L. On the key role of Cu on the oxidation behaviour of Cu−Ni−Fe based anodes for Al electrolysis [J]. Corrosion Science, 2015, 101: 105−113.
[11] GOUPIL G, HELLE S, DAVIS B, GUAY D, ROUÉ L. Anodic behavior of mechanically alloyed Cu−Ni−Fe and Cu−Ni−F−O electrodes for aluminum electrolysis in low-temperature KF−AlF_3 electrolyte [J]. Electrochimica Acta, 2013, 112: 176−182.
[12] GOUPIL G, BONNEFONT G, IDRISSI H, GUAY D, ROUÉ L. Consolidation of mechanically alloyed Cu−Ni−Fe material by spark plasma sintering and evaluation as inert anode for aluminum electrolysis [J]. Journal of Alloys and Compounds, 2013, 580: 256−261.
[13] KHRAMOV A P, KOVROV V A, ZAIKOV Y P, CHUMAREV V M. Anodic behaviour of the $Cu_{82}Al_8Ni_5Fe_5$ alloy in low-temperature aluminium electrolysis [J]. Corrosion Science, 2013, 70: 194−202.
[14] HRYN J, TKACHEVA O, SPANGENBERGER J. Initial 1000A aluminum electrolysis testing in potassium cryolite-based electrolyte [C]//Light Metals. Warrendale, PA: TMS, 2013: 1289−1294.
[15] PADAMATA S K, YASINSKIY A, POLYAKOV P. Anodic process on Cu−Al alloy in KF−AlF_3−Al_2O_3 melts and suspensions [J]. Transactions of Nonferrous Metals Society of China, 2020, 30: 1419−1428.
[16] YASINSKIY A, PADAMATA S K, POLYAKOV P, SAMOILO A, SUZDALTSEV A, NIKOLAEV A. Electrochemical behaviour of Cu−Al oxygen-evolving anodes in low-temperature fluoride melts and suspensions [C]//Light Metals. Warrendale, PA: TMS, 2020: 591−599.
[17] PADAMATA S K, YASINSKIY A, POLYAKOV P. Electrode processes in the KF−AlF_3−Al_2O_3 melts [J]. New Journal of Chemistry, 2020, 44: 5152−5164.
[18] LIN M, HU X W, YU J Y, YANG Y J, LI A M, SHI Z N, WANG Z W. Raman spectroscopy and quantum theory calculations on complexes in the KF−AlF_3−Al_2O_3 system [J]. Journal of Molecular Liquids, 2021, 326: 115267.
[19] YASINSKIY A, SUZDALTSEV A, POLYAKOV P, PADAMATA S K, YUSHKOVA O. Behaviour of aluminium oxide in KF−AlF_3−Al_2O_3 melts and suspensions [J]. Ceramic International, 2020, 46: 11539−11548.
[20] LIU F Q, XIE M Z, LIU W, ZHAO H L. Footprint of harmful substances in spent pot lining of aluminum reduction cell [J]. Transaction of Nonferrous Metals Society of China, 2020, 30: 1956−1963.
[21] HOU W Y, LI H S, LI M, CHENG B J, FENG Y. Effects of electrolysis process parameters on alumina dissolution and their optimization [J]. Transaction of Nonferrous Metals Society of China, 2020, 30: 3390−3403.
[22] WEI W, GENG S J, XIE D B, WANGA F H. High temperature oxidation and corrosion behaviours of Ni−Fe−Cr alloys as inert anode for aluminum electrolysis [J]. Corrosion Science, 2019, 157: 382−391.
[23] DEEPA K, VENKATESH T V. Synthesis and generation of CuO and Mn doped CuO composites and its corrosion behaviour [J]. Materials Today: Proceedings, 2017, 4: 12045−12053
[24] HAMMERL A, WELCH B J, SCHWERDTFEGER P. $F_2Al(\mu\text{-}\eta^2\text{:}\eta^2\text{-}O_2)AlF_2$: An unusual, stable aluminum peroxo compound [J]. Inorganic Chemistry, 2004, 43: 1436−1440.

提高 KF−AlF_3−Al_2O_3 熔体中 Cu−Al 基阳极的耐腐蚀性

Sai Krishna PADAMATA[1], Andrey YASINSKIY[1], Aleksandr SHABANOV[2], Timofey BERMESHEV[1], 杨酉坚[3], 王兆文[3], 曹 导[3], Peter POLYAKOV[1]

1. Laboratory of Physics and Chemistry of Metallurgical Processes and Materials, Siberian Federal University, Krasnoyarsk, Russia;
2. Laboratory of Molecular Spectroscopy, Krasnoyarsk Science Center SB RAS, Krasnoyarsk, Russia;
3. 东北大学 冶金学院，沈阳 110819

摘　要：采用恒电流和动电位极化技术研究经预氧化的和未经预氧化的 Cu−Al 基阳极(Cu−10Al 和 Cu−9.8Al−2Mn)在 KF−AlF_3−Al_2O_3 熔体中的阳极行为。将合金在 700 °C 下进行短时间(8 h)氧化，然后在 800 °C 下施以 0.4 A/cm^2 的电流密度进行 1 h 恒电流极化。测定扫描速率为 0.01 V/s 的动电位曲线。对在阳极表面冻结的熔体样品进行 XRD 分析，并在实验后对阳极进行 SEM 分析，以研究合金表面形成的氧化皮的物相。所有阳极材料的稳态电位都在 2.30~2.50 V(vs Al/AlF_3)范围内。根据动电位极化获得的数据计算阳极的腐蚀速率。结果表明，经预氧化的阳极比未经预氧化的阳极具有更低的腐蚀速率。

关键词：惰性阳极；钾冰晶石；Cu−Al 合金；腐蚀；铝电解；析氧电极

(Edited by Wei-ping CHEN)